INTERNATIONAL ATOMIC ENERGY AGENCY
UNITED NATIONS EDUCATIONAL, SCIENTIFIC AND CULTURAL ORGANIZATION
INTERNATIONAL CENTRE FOR THEORETICAL PHYSICS
I.C.T.P., P.O. BOX 586, 34100 TRIESTE, ITALY, CABLE: CENTRATOM TRIESTE

H4.SMR/782-9

Second Workshop on
Three-Dimensional Modelling of Seismic Waves
Generation, Propagation and their Inversion

7 - 18 November 1994

A Comparative Study of Source Processes by Surface Waves Inversion and Analysis of Aftershock Data

B.G. Bukchin

International Institute of Earthquake Prediction
Theory and Mathematical Geophysics
Russian Academy of Sciences
Moscow, Russian Federation

A COMPARATIVE STUDY OF SOURCE PROCESSES BY SURFACE WAVES INVERSION AND ANALYSIS OF AFTERSHOCK DATA

B. G. Bukchin

International Institute of Earthquake Prediction Theory and Mathematical Geophysics, Russian Academy of Sciences

SURFACE WAVES INVERSION

In this section I will remind you the main definitions from my lectures at the Workshop 1992.

Stress glut moments of total degree 2 determine the geometry, duration of a seismic source and the propagation of rupture. Following Backus and Mulcahy, 1976 we will define the source region as a region occupied by nonelastic motion, or the region where the partial derivative of the stress glut tensor with respect to the time $\dot{\Gamma}_{ij}$ is not identically zero.

We will consider a special case of a seismic source where the stress glut tensor can be expressed by the equation

$$\dot{\Gamma}(\mathbf{x},t) = f(\mathbf{x},t)\mathbf{M}, \tag{1}$$

where $f(\mathbf{x},t)$ is a nonnegative scalar function and $\mathbf{M}$ is a normalized seismic moment tensor. In this case the source region can be defined by the condition that $f(\mathbf{x},t)$ is not identically zero and the source duration is the time during which inelastic motion occurs at various points within the source region, i.e., $f(\mathbf{x},t)$ is different from zero. Spatio-temporal characteristics of the source can be expressed by corresponding moments of the function $f(\mathbf{x},t)$. In the general case stress glut moments of spatial

degree 2 and higher are not uniquely determined by the displacement field. But in the case when equation (1) is valid such a uniqueness takes place (see appendix 1).

The following equations express the integral estimates of the source characteristics in terms of spatio-temporal moments of $f(\mathbf{x},t)$ of total degree (both in space and time) 0, 1, and 2.

The moment $\mathbf{f}^{(m,n)}(\mathbf{q},\tau)$ of spatial degree m and temporal degree n with respect to point $\mathbf{q}$ and instant of time τ is a tensor of order m and is given by the formula $(k_1,\dots,k_m = 1,2,3)$

$$f^{(m,n)}_{k_1\dots k_m}(\mathbf{q},\tau) = \int_\Omega dV_x \int_0^\infty f(\mathbf{x},t)(x_{k_1}-q_{k_1})\dots(x_{k_m}-q_{k_m})(t-\tau)^n dt. \tag{2}$$

Source location is estimated by the spatial centroid $\mathbf{q}_c$ of the field $f(\mathbf{x},t)$ defined as

$$\mathbf{q}_c = \mathbf{f}^{(1,0)}(0)/M_0, \tag{3}$$

where $M_0 = f^{(0,0)}$ is the scalar seismic moment. In a similar fashion, the temporal centroid τ_c is estimated by the formula

$$\tau_c = f^{(0,1)}(0)/M_0. \tag{4}$$

The source duration is Δt estimated by $2\Delta\tau$, where

$$(\Delta\tau)^2 = f^{(0,2)}(\tau_c)/M_0. \tag{5}$$

Let $\mathbf{r}$ be a unit vector. The mean source size along $\mathbf{r}$ is estimated by $2l_r$, where

$$l_r^2 = \mathbf{r}^T\mathbf{W}\mathbf{r} \tag{6}$$

and

$$\mathbf{W} = \mathbf{f}^{(2,0)}(\mathbf{q}_c)/M_0. \tag{7}$$

From (7) it follows that the source region has the least mean size along that eigenvector of **W** corresponding to the least eigenvalue and the greatest mean size along that eigenvector of the same matrix corresponding to the greatest eigenvalue. Let **v** be the mean velocity of the instant spatial centroid (see Bukchin B.G., 1989). Then

$$\mathbf{v} = \mathbf{w}/(\Delta\tau)^2, \tag{8}$$

where

$$\mathbf{w} = \mathbf{f}^{(1,1)}(\mathbf{q}_c, \tau_c)/M_0.$$

The relation between the spectrum of the displacement field $u_i(\mathbf{x},\omega)$ and the spatio-temporal moments of the function $f(\mathbf{x},t)$ can be expressed by the formula (see appendix 1)

$$u_i(\mathbf{x},\omega) = \sum_{m=0}^{\infty}\sum_{n=0}^{\infty}\frac{(-1)^n}{m!n!} f^{(m,n)}_{k_1\ldots k_m}(0,0)M_{jl} \times (i\omega)^{n-1}\frac{\partial}{\partial y_{k_1}}\cdots\frac{\partial}{\partial y_{k_m}}\frac{\partial}{\partial y_l}G_{ij}(\mathbf{x},\mathbf{y},\omega)\mid_{y=0} \tag{9}$$

(the summation convention for repeated subscripts is used). Here we assume that the point $\mathbf{y} = 0$ and the instant $t = 0$ belong to the source region and the time of the source activity respectively. $G_{ij}(\mathbf{x},\mathbf{y},\omega)$ is the spectrum of the Green function for the chosen model of medium and wave type (see Levshin, 1985). Since (9) involve infinite series, these relations cannot be used to compute the moments $\mathbf{f}^{(m,n)}$. However, when the displacement function $u_i(\mathbf{x},\omega)$ and the Green function $G_{ij}(\mathbf{x},\mathbf{y},\omega)$ have been low pass filtered, the terms in (9) start to decrease with m and n increasing (see Backus, 1977) at least as rapidly as $(\omega\Delta t)^{m+n}$ ($\omega\Delta t < 1$; Δt - the source duration) and one might then restrict oneself to considering finite sums only. Representing in this form the spectrum of displacements in surface waves, we can derive a set of equations for the moments of f of total degree $m + n \le N$.

Let us consider a low frequency part of the spectrum of the $i-th$ component of displacements carried by some Love or Rayleigh mode $u_i(\mathbf{x},\omega)$. If the frequency ω is small (the time duration of the source is much smaller than a period, and the size of the source region is much smaller than a wave length), then we can take into account in formula (9) only the first terms for $m + n \le 2$.

Let $\mathbf{y} = 0$ - position of spatial centroid of the source and $t = 0$ - temporal centroid. Then we have $f^{(1,0)} = f^{(0,1)} = 0$. In this case (9) can be written as follows

$$\begin{aligned} u_i(\mathbf{x},\omega) = {} & \frac{1}{i\omega}M_0M_{jl}\frac{\partial}{\partial y_1}G_{ij}(\mathbf{x},\mathbf{y},\omega)\mid_{y=0} \\ & + \frac{1}{2i\omega}f^{(2,0)}_{mn}(0,0)M_{jl}\frac{\partial}{\partial y_m}\frac{\partial}{\partial y_n}\frac{\partial}{\partial y_l}G_{ij}(\mathbf{x},\mathbf{y},\omega)\mid_{y=0} \\ & - f^{(1,1)}_{m}(0,0)M_{jl}\frac{\partial}{\partial y_m}\frac{\partial}{\partial y_l}G_{ij}(\mathbf{x},\mathbf{y},\omega)\mid_{y=0} \\ & + \frac{i\omega}{2}f^{(0,2)}(0,0)M_{jl}\frac{\partial}{\partial y_l}G_{ij}(\mathbf{x},\mathbf{y},\omega)\mid_{y=0}. \end{aligned} \tag{10}$$

If all characteristics of the medium, depth of the best point source and seismic moment tensor are known (determined, for example, using the spectral domain of longer periods) the representation (10) gives us a system of linear equations for moments of the function f of total degree 2. Let us consider a plane source. All moments of f of total degree 2 can be expressed in this case by formulas (3)–(8) in terms of 6 parameters: Δt - estimate of source duration, $l_{\max}$ - estimate of maximal mean size of the source, φ_l - estimate of the angle between the direction of maximal size and strike axis, $l_{\min}$ - estimate of minimal mean size of the source, v - estimate of the absolute value of instant centroid velocity **v** and φ_v - the angle between **v** and strike axis.

Using the Bessel inequality for the moments under discussion we can obtain the following constrain for the parameters considered above (see appendix 2)

$$v^2\Delta t^2(\cos^2\varphi/l^2_{\max} + \sin^2\varphi/l^2_{\min}) \le 1. \tag{11}$$

Here φ – the angle between direction of maximal size and direction of v. Assuming that the source is a plane fault and representation (1) is valid let us consider a rough grid in the space of 6 parameters defined above. These parameters have to follow (11). Let models of the media be given and the moment tensor be fixed as well as the depth of the best point source. Let the fault plane (one of two nodal planes) be identified. Using formula (10) we can calculate the amplitude spectra of surface waves at the points of observation for every possible combination of values of the varying parameters. Comparison of calculated and observed amplitude spectra give us a residual $\varepsilon^{(i)}$ for every point of observation, every wave and every frequency ω. Let $u^{(i)}(\mathbf{r},\omega)$ be any observed value of the spectrum, $i = 1,\ldots,N$; $\varepsilon^{(i)}$ – corresponding residual of $|u^{(i)}(r,\omega)|$. We define the normalized amplitude residual by formula

$$\varepsilon(\Delta t, l_{\max}, l_{\min}, \varphi_l, v, \varphi_v) = [(\sum_{i=1}^{N} \varepsilon^{(i)2})/(\sum_{i=1}^{N} |u^{(i)}(\mathbf{r},\omega)|^2)]^{1/2}. \qquad (12)$$

Fixing the value of one of varying parameters we will put in correspondence to it a minimal value of the residual ε on the set of all possible values of the other parameters. In this way we will define 6 functions of the residual corresponding to the 6 varying parameters: $\varepsilon_{\Delta t}(\Delta t), \varepsilon_{l_{\max}}(l_{\max}), \varepsilon_{l_{\min}}(l_{\min}), \varepsilon_{\varphi_l}(\varphi_l), \varepsilon_v(v)$ and $\varepsilon_{\varphi_v}(\varphi_v)$. The value of the parameter for which the corresponding function of the residual attains its minimum we will define as estimate of this parameter. At the same time these functions characterize the degree of resolution of the corresponding parameters.

Following example illustrates the technique described above. Using this technique we estimated the characteristics of the Georgian earthquake, 23.10.92 ($M_b = 6.1, M_s = 6.5$). This research was conducted in collaboration with R.Madariaga and J.M.Gomez. The estimation of source parameters was done by using spectra of Love and Rayleigh fundamental modes in the spectral domain 35 to 150s. The distribution of stations is shown in Figure 1.

Love and Rayleigh fundamental modes were extracted by using a frequency-time analysis program (FTAN). Figures 2-5 illustrate FTAN processing of 3-component HRV (Harvard) broad band seismogram. As one can see from Figure 5, amplitude spectrum of the signal extracted by floating filtration in the band $30s < T < 150s$ is much more smooth than spectrum of the record just filtered in the same band. It makes the inversion much more stable.

Analyzing the long period part of the spectra (periods from 60 to 150 seconds) we determined the following focal mechanism of the source: strike 300°, dip 15° and rake 135°. The stereographic projection of nodal planes on the lower hemisphere is shown in Figure 6a. The estimate of seismic moment is $4.8 \cdot 10^{18} n \cdot m$. The best point source depth was found to be about 16 km - the amplitude spectra residual as function of the best point source depth is shown in Figure 7. This results are in a good agreement with Harvard's solution presented in Figure 6b.

To estimate duration and geometry of the source we have used amplitude spectra of fundamental modes of Love and Rayleigh waves in the spectral domain from 35 to 50 seconds. The plane dipping to the North was identified as a fault plane. Results of direct trial of possible values of the unknown parameters are shown in the Figure 8. $\varepsilon_{\Delta t}$ attains its minimum at the value of duration equal to 6s. The value $v = 3.2km/s$ corresponds to the minimum of ε. Residuals $\varepsilon_{l_{\max}}$ and $\varepsilon_{l_{\min}}$ as functions of maximal mean size of the source $l_{\max}$ and minimal mean size $l_{\min}$ respectively give us the following estimates $l_{\max} = 32km$ and $l_{\min} = 20km$. The functions ε_{φ_l} and ε_{φ_v} defining direction of maximal mean size of the source and direction of the instant centroid velocity - two last curves in Figure 8. These residuals were calculated for all possible values of angles φ_l and φ_v while other parameters were fixed equal to their estimates obtained before. Angles are measured in the foot wall of the fault plane clockwise round from the strike axis. φ_l varies from 0° to 180°, φ_v – from 0° to 360° and attain

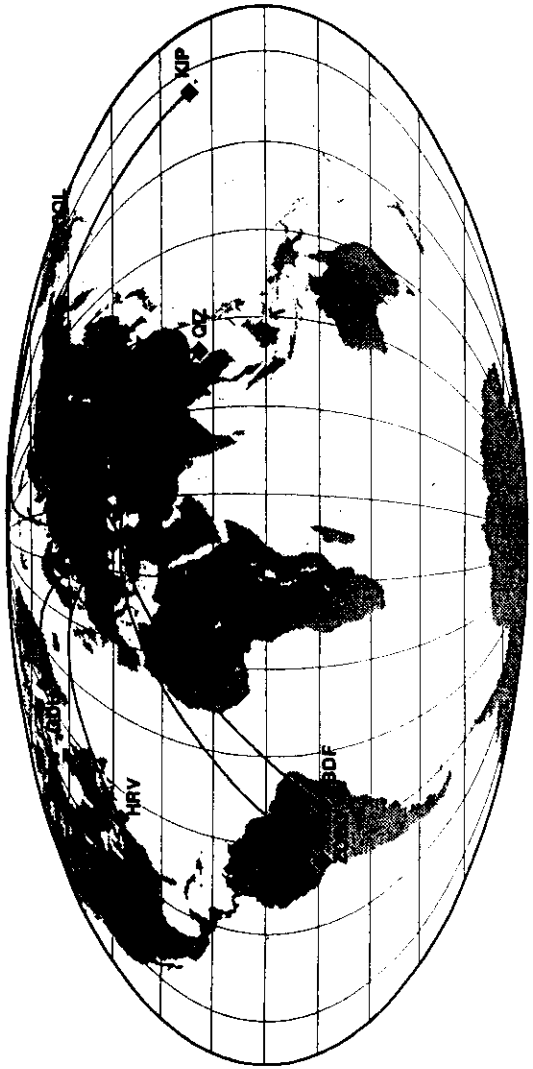

Fig.1. Station distribution.

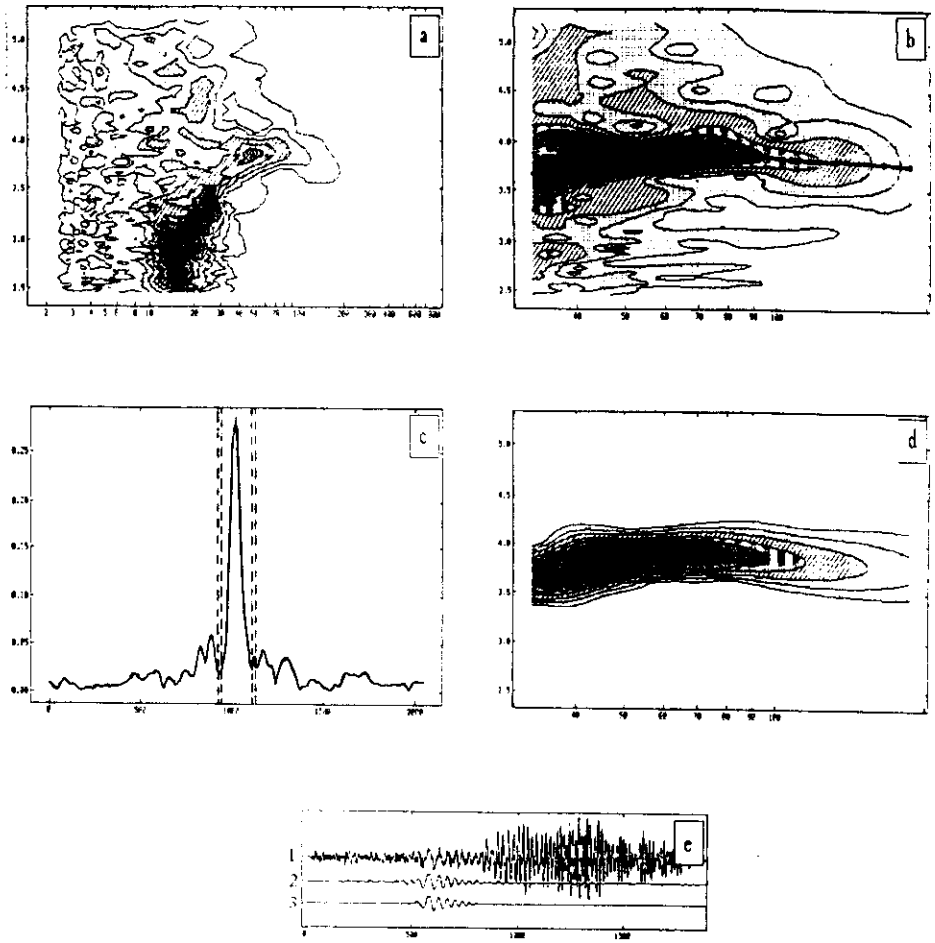

Fig.2. FTAN processing of HRV vertical component.
(a) - FTAN diagram of original record; (b) - FTAN diagram of record filtered in the band of periods from 30 to 150 seconds and dispersion curve used for phase equalisation; (c) - record envelope after phase equalisation and filtration in time domain (floating filtration); (d) - FTAN diagram after floating filtration; (e) - comparison of records: 1 - original, 2 - filtered in the band 30s<T<150s, 3 - after floating filtration.

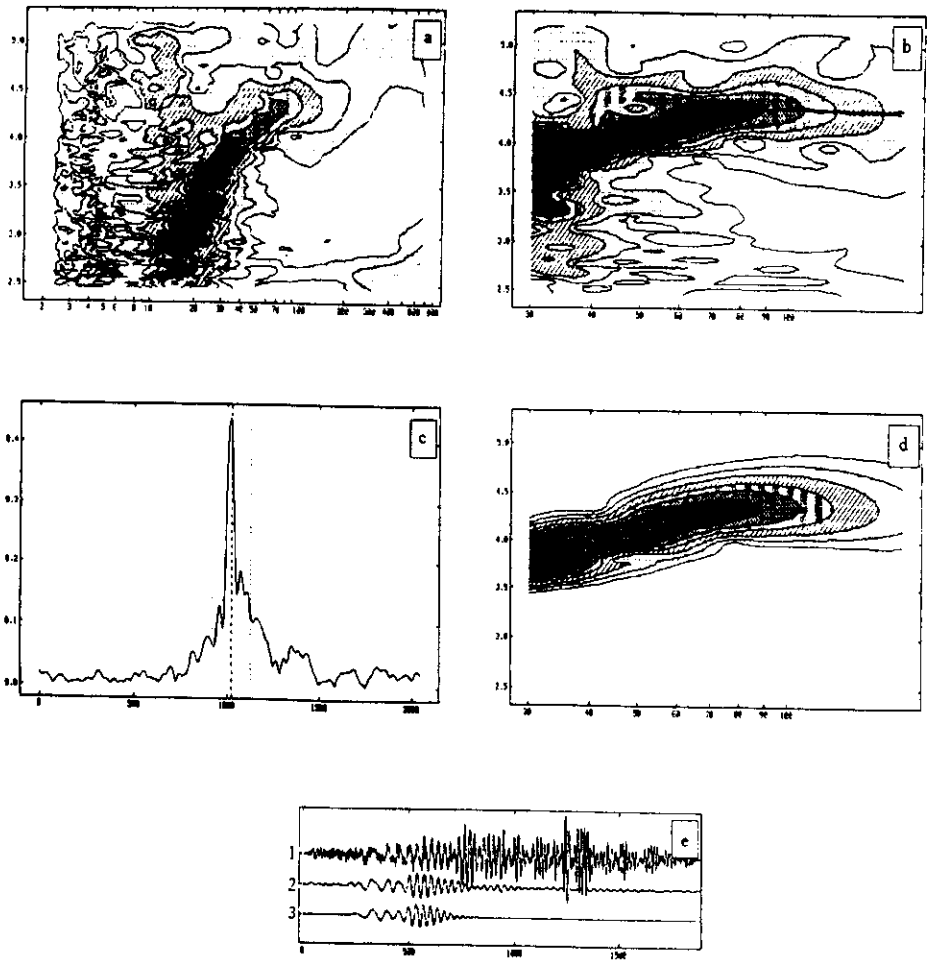

Fig.3. FTAN processing of HRV transversal component.
(a) - FTAN diagram of original record; (b) - FTAN diagram of record filtered in the band of periods from 30 to 150 seconds and dispersion curve used for phase equalisation; (c) - record envelope after phase equalisation and filtration in time domain (floating filtration); (d) - FTAN diagram after floating filtration; (e) - comparison of records: 1 - original, 2 - filtered in the band 30s<T<150s, 3 - after floating filtration.

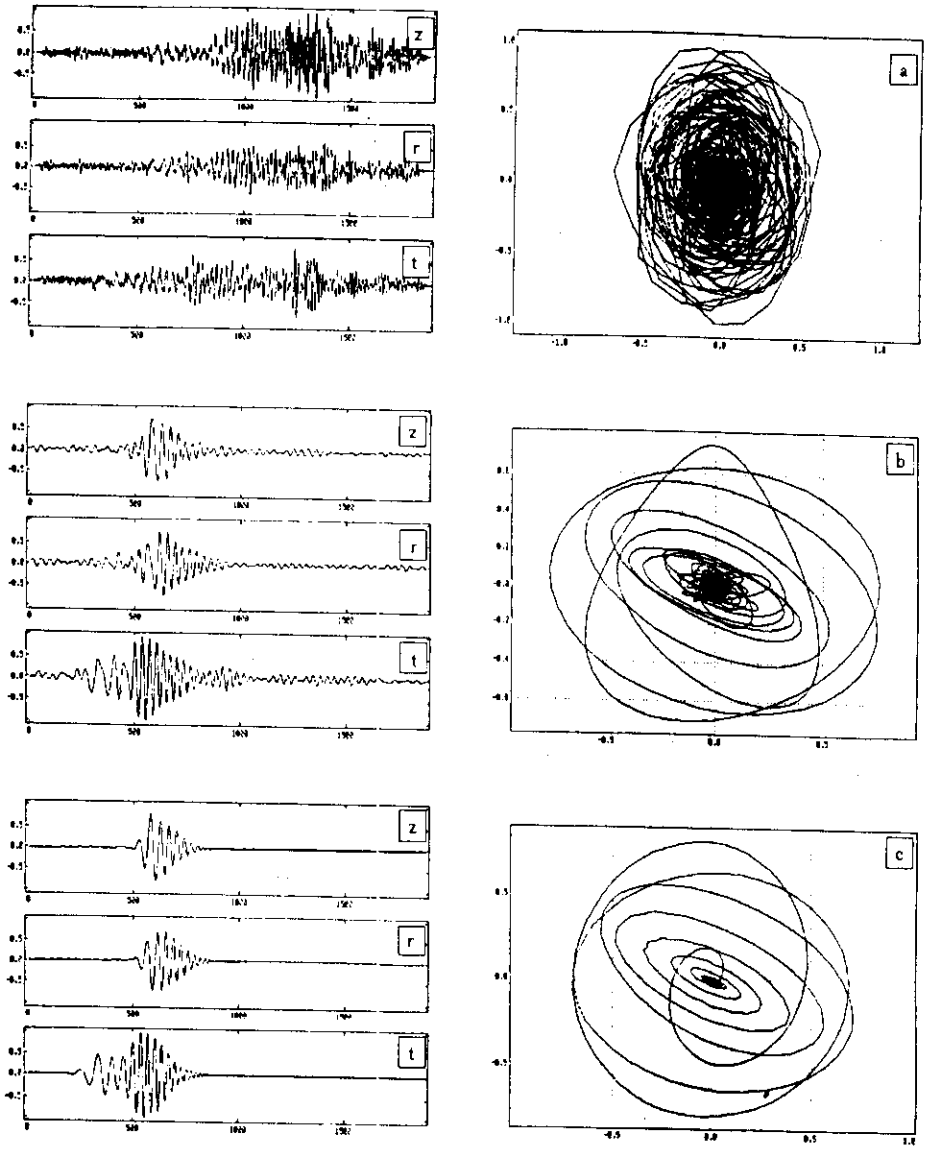

Fig.4.

3-component seismograms and particle motion in z-r plane. a - original records; b - records filtered in the band of periods 30s<T<150s; c - result of floating filtration.

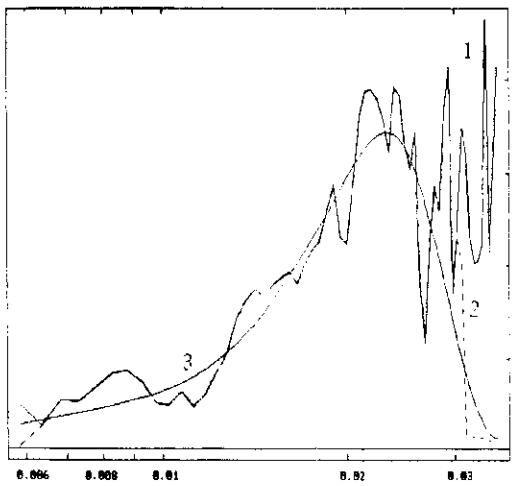

Fig.5. Amplitude spectra of HRV vertical component.

1 - original, 2 - after filtering in the band 30s<T<150s,
3 - after floating filtration.

(a)

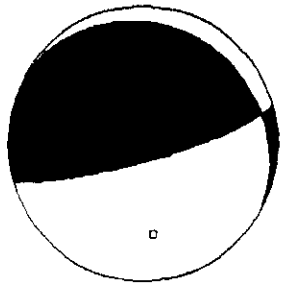

Focal mechanism from long period Love and Rayleigh waves inversion. M0 = 0.48*10**19 h m. Depth = 15 km.

(b)

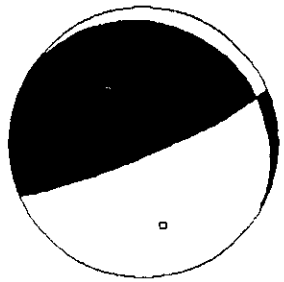

Harvard's focal mechanism. M0 = 0.5*10**19 h m.
Depth = 16 km.

Fig.6.

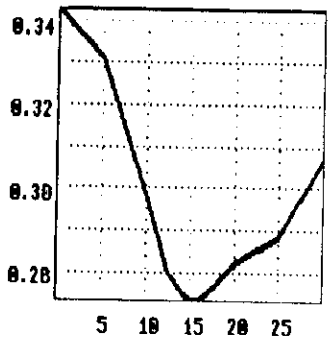

Fig.7.

Amplitude spectra residual as function of depth.

Fundamental Love and Rayleigh waves in the band of periods from 60 to 150 seconds are used.

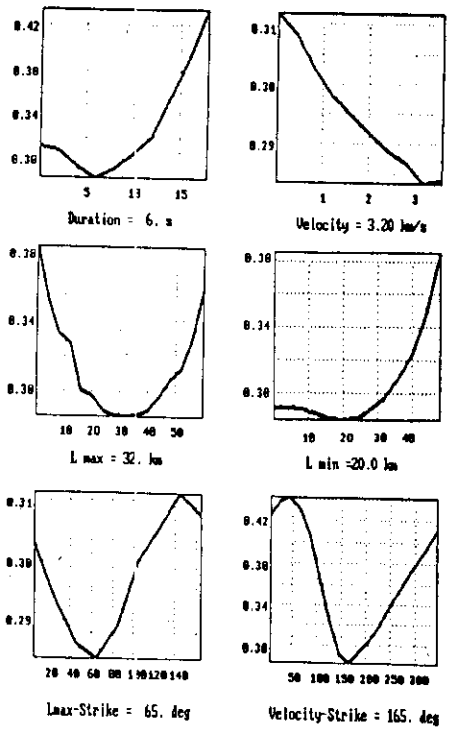

Fig.8.

Residuals as functions of varied parameters.

The value of the parameter for which correspondent function of the residual attains its minimum is defined as estimate of this parameter.

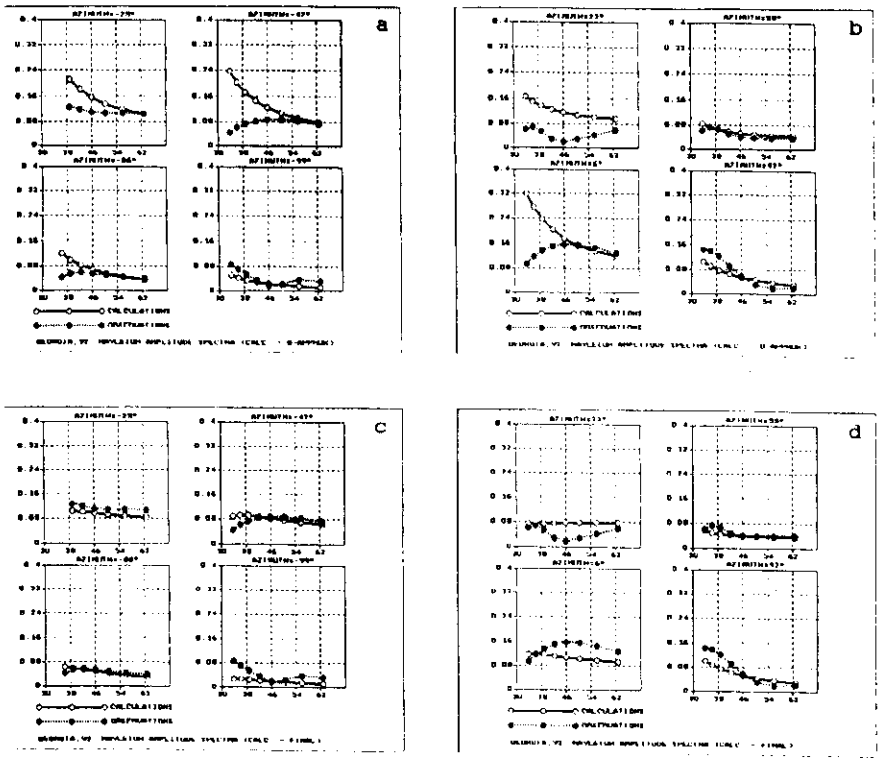

Fig.9.

Comparison of synthetic and observed Rayleigh waves' short period amplitude spectra (34s < T < 63s).

(a), (b) - synthetic spectra in approximation of instant point source;
(c), (d) - synthetic spectra in approximation of stress glut' 2-nd moments.

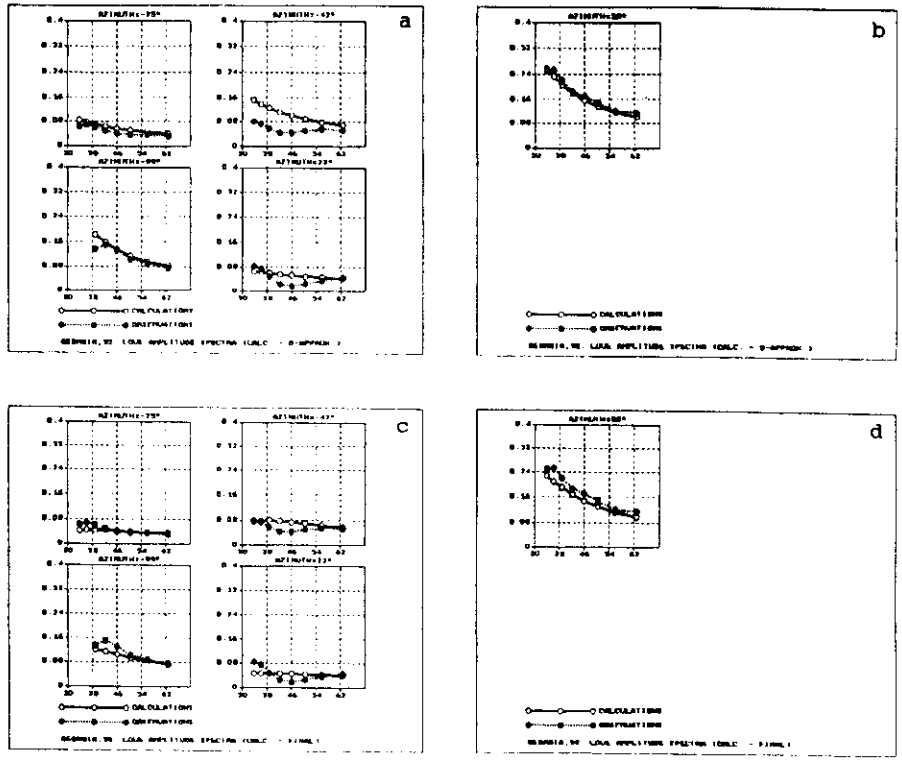

Fig.10.

Comparison of synthetic and observed Love waves' short period amplitude spectra (34s < T < 63s).

(a), (b) - synthetic spectra in approximation of instant point source;
(c), (d) - synthetic spectra in approximation of stress glut' 2-nd moments.

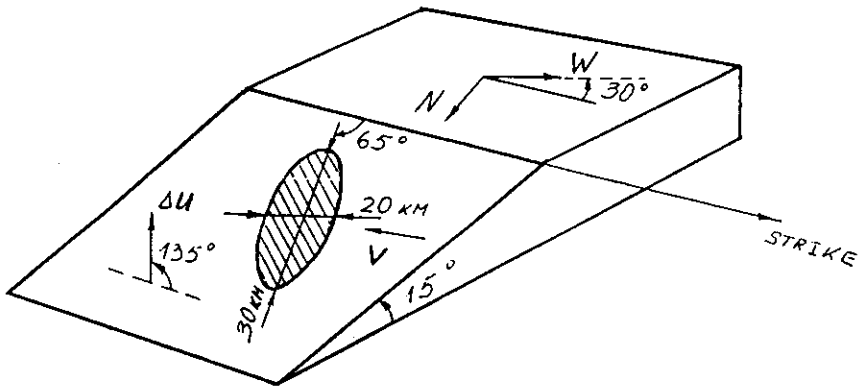

Fig.11. Focal mechanism and integral source parameters. ΔU-slip vector. V-velocity of instantaneous centroid.

their minima at the angles 65° and 165° respectively.

Comparison of synthetic and observed short period amplitude spectra of Rayleigh and Love waves is shown in Figures 9 and 10. The stations are marked in the figures by azimuthes from the epicenter to the stations. Synthetic spectra given in Figures 9a, 9b and 10a, 10b were calculated in approximation of an instant point source. Synthetic spectra given in Figures 9c, 9d and 10c, 10d were calculated in approximation (10) using stress glut' 2-nd moments. Comparison of figures (a,b) with figures (c,d) shows that the amplitude spectra fitting is better significantly in the case of approximation (10).

As a result of surface wave spectra analysis we produced a model of the source which is given in Figure 11. The ellipse represents here the integral estimates of source geometry. $\Delta\mathbf{U}$ – slip vector, $\mathbf{V}$ – direction of the instant centroid velocity.

RECONSTRUCTION OF STRAIN FIELDS FROM AFTERSHOCK DATA

In this section a brief description of the strain fields reconstruction technique is given.

1. Given first motion observations for an earthquake (subscript k), these data are used 1971] to compute the likelihood function l of a normalized strain tensor m (treated as a vector in a five-dimensional linear space of three-dimensional symmetrical vectors with zero trace) and the posterior probability density

$$P_k(\mathrm{m}) = l(\mathrm{m}) / \int l(\mathrm{m}) d\mathrm{m}$$

Here and below, any integral (replaced by a sum in calculations) is approximately computed on a five-dimensiona unit sphere.

The density is used to find the mean value of the tensor and the covariance error matrix of its components

$$\langle \mathbf{m} \rangle_k = \int \mathbf{m} P_k(\mathbf{m}) d\mathbf{m}; \qquad \mathbf{B}_k = \int \mathbf{m}\mathbf{m}^{\mathrm{T}} P_k(\mathbf{m}) d\mathbf{m} - \langle \mathbf{m} \rangle_k \langle \mathbf{m} \rangle_k^{\mathrm{T}}$$

2. The strain amplitude at the hypocenter is assumed to be independent of the magnitude M_k, but the relevant strain $\mathbf{m}$ described by the probability distribution $P_k(\mathbf{m})$ is ascribed to a volume surrounding the kth hypocenter $\mathbf{r}_k$ whose characteristic radius is defined by

$$\lg R_k = \mathrm{M}_k/2 + \mathrm{const}$$

The strain amplitude smoothly falls off from the center to the edges of the volume according to the law $D((\mathbf{r} - \mathbf{r}_k)/R_k)$ whose form is specified by our prior knowledge of the structure of the area and available data.

3. Assuming the $\mathbf{m}_k$ for different earthquakes to be independent, one finds the total strain at an arbitrary point $\mathbf{r}$ as

$$\mathbf{M}(\mathbf{r}) = \sum_k D((\mathbf{r} - \mathbf{r}_k)/R_k) \langle \mathbf{m} \rangle_k,$$

and the "error matrix" as

$$\mathbf{B}(\mathbf{r}) = \sum_k D((\mathbf{r} - \mathbf{r}_k)/R_k) \mathbf{B}_k.$$

The strain amplitude at $\mathbf{r}$ is defined to be the absolute value of the five-dimensional vector $|\mathbf{M}(\mathbf{r})|$.

The uncertainty is estimated, in particular, by using the typical signal/noise ratio

$$q(\mathbf{r}) = \{|\mathbf{M}(\mathbf{r})|/[\mathrm{Trace}\{\mathbf{B}(\mathbf{r})\}/5]\}^{1/2}.$$

4. Horizontal strain on the horizontal plane is given by the tensor $\mathbf{h}(2 \times 2)$, which is a minor of the total strain tensor $\mathbf{M}$ (in matrix form) in the relevant basis.

The tensor $\mathbf{h}$ has a nonzero trace in the general case, where areas of compression (Trace $\mathbf{h} < 0$) and extension (Trace $\mathbf{h} > 0$) exist in the horizontal plane. From the

requirement Trace $\mathbf{M} = 0$ it follows that the value of Trace $\mathbf{h}$ taken with the opposite sign is equal to the vertical strain component of the horizontal plane. For this reason areas of general horizontal compression in this model are also zones of subsidence, and areas of extension are zones of uplift.

AN EXAMPLE OF COMPARATIVE STUDY OF SOURCE PROCESSES BY SURFACE WAVES INVERSION AND ANALYSIS OF AFTERSHOCK DATA

We will consider the Khailino earthquake, 1991 (Koryakia, North-Eastern Asia). The event occurred at 11h 36min 28.4s with coordinates 60.90°N, 167.02°E and depth 13 km, $M_s = 6.5$. The results of this earthquake study were described by Lander A.V. et al., 1994. In this paper you can find geological and tectonic aspects of this study. Here we will discuss the application of the techniques described above. The earthquake was accompanied by considerable aftershock (sixty-two events with $M \geq 4$, twenty-two of these being with $M \geq 5$) activity recorded within about four months. There was a short-lived aftershock burst about 45 days following the main shock and localized about 10 km southwest of the mainshock epicenter. A single $M = 4.5$ aftershock was recorded within a year of June 1991, and a sequence of three $M = 4.5$ events occurred at the same location within an hour in July 1992. All hypocenters were crustal, but no satisfactory depth determinations are available. For this reason it is only the distribution of epicenters which is amenable to interpretation. The aftershock area with characteristic dimensions of 60x30 km has an overall northwest elongation.

The main shock was recorded by many stations of the world digital networks, so that the source parameters could be estimated from long period surface wave spectra. The source parameters listed below (see Figure 12) were derived using the technique described above as applied to Rayleigh and Love fundamental modes recorded at 12

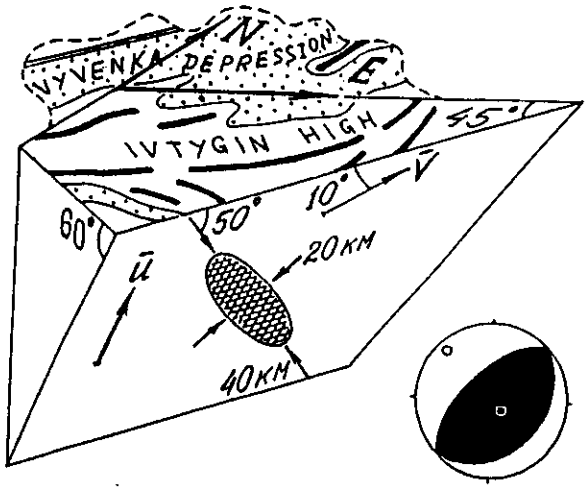

Fig. 12. Focal mechanism and integral source parameters for the main shock based on surface wave data. U-slip vector. V-velocity of instantaneous centroid.

stations within the period range 30 to 200 s :

- seismic moment 1.3×10^{26} dyne cm ;

- focal mechanism (preferred plane): strike azimuth 225°, dip 60° , rake 90° (reverse slip);

- parameters of second time-space moments on the focal plane (the source is assumed to be a plane, the angles are measured from the strike axis counterclockwise): total duration 6–8 s, greater source dimension 40 km, smaller dimension 20 km; the direction of the greater axis is 50°, the absolute velocity of the instantaneous centroid is 3.3 km s^{-1}, the direction of centroid motion is 170°.

The seismic moment tensor was determined for the periods 70 to 200 s, the range being 30–60 s for the second moments.

Body wave first motions were known for the main shock, a foreshock, and 46 aftershocks. Most focal mechanism solutions have low likelihood values, being inconsistent with the double couple hypothesis. Nevertheless, one can identify trends in the spatial strain distribution within the source zone by combining data for near aftershocks. Below we discuss strain fields for the aftershocks obtained by the technique described above. The principal effects observed in the strain fields have a ratio of amplitude to typical error within 0.5–2.0, hence the results can be treated as merely indicating some qualitative trends.

The earthquake source zone, or to be more specific, the area involved in the aftershock process, completely lies in the part of the Kamchatka terrain separated by the Ivtygin high. The main shock and the larger aftershocks (18 out of 23 with $M \geq 5.0$) occurred close to the northwestern Ivtygin slopes, partly within the high. The aftershocks in the Vyvenka depression have significantly lower magnitudes (a single event with $M > 5$).

The aftershock area has a shape that is obviously inconsistent with the general

structural pattern of the region. The area (Figure 13)[1] has an overall northwest elongation across the general trend and traverses the Vyvenka depression and adjacent higher areas. Note that the longer axis of the aftershock area is close to the axis of symmetry of the Ivtygin arc.

The internal structure of the aftershock area does not repeat the outer outline. The epicenters are denser in a north-south 50x15-km band that becomes broader near the mainshock epicenter (Figure 13). This picture is not in agreement with any visible geologic feature. Since hypocenter depths are subject to some uncertainty, the aftershocks cannot possibly be related to a definite side of the main fault. Overall, however, the southern part of the north-south band generally lies in the area which is frontal with respect to the main fault of the region, whereas the northern part is in the back part.

To sum up, three typical directions are identified within the rupture zone corresponding to features of differing dimensions:

- the northeast trend of major geologic features;
- the northwest trend of the aftershock area as a whole;
- the nearly north-south trend of the denser aftershock epicenters.

Each direction is also present in the seismogram-based parameters of the mainshock source in the averaging scale of the technique:

- the long period estimates of the mainshock focal mechanism are consistent with slip on a northeast fault dipping landward (Figure 12);
- the horizontal slip component is parallel to the aftershock area, which in turn coincides with the direction of the axis of symmetry for the Ivtygin high;
- the north-south directions in the inner aftershock area structure correlate with the

[1] Figures 13 through 15 are given in a kilometer cartesian system with the origin at the mainshock epicenter.

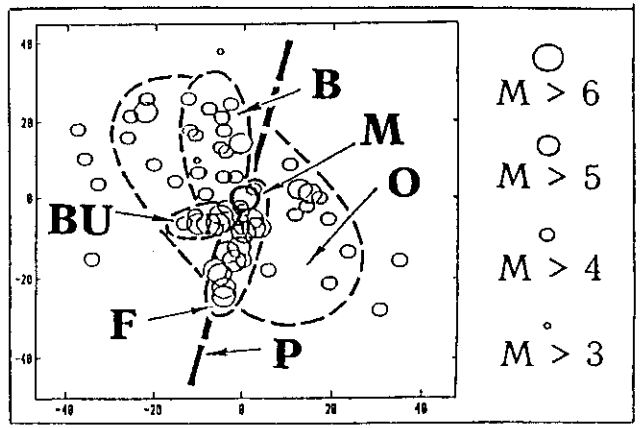

Fig. 13. Aftershock area Elements of the aftershock area mentioned in main text: M-main shock; O-aftershock area outline; F, B, BU-north-south dense aftershock band (F-frontal cluster, B-cluster in the back of the main rupture, BU-aftershocks associated with the burst of activity 15 days following the main shock). P-Direction of the horizontal projection made by the major axis of the ellipse fitting the main rupture (based on instrumental observations).

shape of the main rupture, or more precisely, with the direction of the horizontal projection made by the longer axis of the ellipse that fits the main rupture (Figure 13), but the overall length of the north-south aftershock band is more than twice the projection size.

Estimation of seismogenic strain fields in the aftershock process reveals the following trends.

The largest deformation occurred in the frontal (with respect to the main rupture) part of the source area (Figure 14). Note that this result is not a direct consequence of larger aftershock magnitudes in the southern part of the rupture zone, but also implies a certain similarity in the focal mechanisms.

The rupture zone divides into several significantly different areas by the character of strain (Figure 15). In particular, the north-south group of aftershocks clearly separates into two bands situated en echelon around the mainshock epicenter. The southern (frontal) band coincides with the area of largest strain. It deviates eastward from north-south, approaching the general Ivtygin trend. The northern (back) band which is wholly within the Vyvenka depression consists of smaller aftershocks, and trends north-south. While being different in the character of strain, the interiors of the two bands are reasonably homogeneous. An exception is the cluster of aftershocks southwest of the epicenter, which occupies an intermediate place both spatially and by the character of strain. The aftershocks are a burst of activity that took place 45 days following the main shock, and must apparently be treated as an independent episode associated with another major rupture. One also identifies an area in the northwestern side of the Vyvenka depression where the strain is similar to that in the frontal band.

The tectonic process in the rupture zone can be vividly presented in terms of strain on the horizontal plane. The southern frontal band was dominated by horizontal

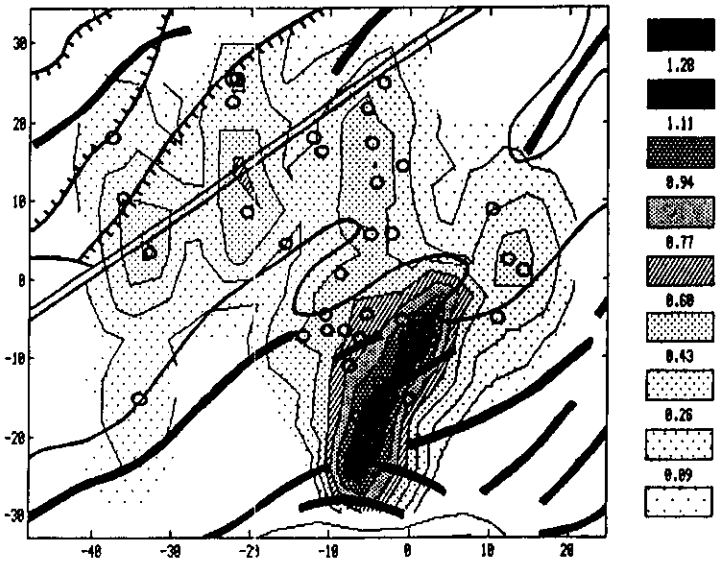

Fig. 14. Map showing the spatial distribution of strain amplitudes in the aftershock process (in arbitrary units). Also some elements of the structural plan of the area are shown, circles marking the epicenters of aftershocks used to deduce the strain.

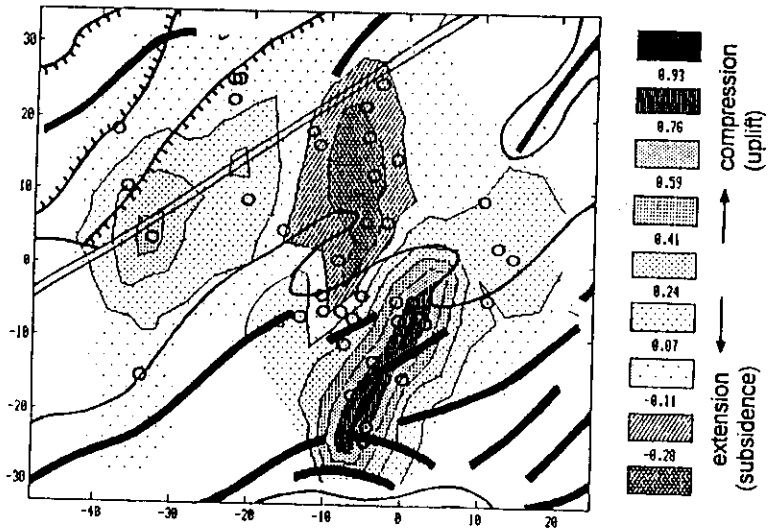

Fig. 15. Map showing areas of overall uplift and subsidence (overall horizontal compression and extension). The units are arbitrary.

compression or uplift during the aftershock process (the two statements are identical in the model adopted here). In contrast to this, there was extension or subsidence going on in the northern band (Figure 15). It is interesting to note that the coseismic strain correlates well with tectonic structure and topography, even within a single rupture zone. The higher southeastern and northwestern margins of the zone are dominated by compression and the Vyvenka depression by extension.

The vector of largest horizontal strain (compression in our case) in the frontal band has virtually the same direction as the aftershock band itself. Thus, most of aftershock slip at the location took place along the band. Now that direction is also in agreement with the instrumental estimate of major axis for the ellipse fitting the main rupture. Combining the last three observations, one concludes that most of the slip in the part of aftershock area under discussion took place on the mainshock fault.

The effect is not as well defined in the northern band. Although the largest horizontal strain (extension) differs from the north-south trend of the band by 20 degrees only, the difference from the most likely direction of extension in the Vyvenka depression is the same . It is not clear what alternative should be preferred, considering the low quality of the data.

The spatial and strain parameters of the aftershock process exhibit definite correlations with the instrumental estimates of the mainshock rupture shape (Figures 12 through 15). The resulting fault seems to control the strength anisotropy of the ruptured volume after the main shock. The strength limit (friction) on the fault plane was lower than in the surrounding rock, and the material began to "flow" along the weakened zone. The flow was recorded as the aftershock band aligned along the major axis of the fault-fitting ellipse.

It has been mentioned above that the most active (11 events out of 23 with $M \geq 5$) frontal set of aftershocks in the southern part of the rupture zone (this is the

area of largest strain) best fits this model when strain characteristics are considered. Its length (20 km) is also consistent with the instrumental estimate of the major fault axis as projected onto the ground surface. Hence the main rupture most likely took place in the southeastern part of the source zone. The spatial identification of the main rupture and the frontal aftershocks means that the fault plane intersects the ground surface within the Ivtygin high. For this reason, even though the main shock and most aftershocks occurred in the depression, the main earthquake seems to have been located in the southern Ivtygin high.

The fact that the secondary flow was confined to the mainshock plane is not so unexpected in itself. The peculiarity of the present situation is that the fault is glaringly discordant with respect to all principal source mechanism directions. As a result, the secondary flow occurred at an angle of about 40 degrees with the main rupture. Note that the observed flow direction (southward, which is consistent with the frontal compression) coincides with the projection of the main slip onto the major fault axis.

The sharp change in the source strength anisotropy suggests that the Khailino rupture is a new formation rather than a segment of a long-existing fault. This is all the more evident from the distribution of strain during the aftershock process. The aftershock area is much larger than the area of mainshock coseismic excitation. However, the above pattern of secondary flow was observed around the main rupture alone. Far from the rupture the strain is essentially different (Figure 15), that is, the strain fields obtained do not show any extension of the rupture, let alone the excitation of a major fault that is typical of many large earthquakes. We remind that neither is such rupture identified in the visible tectonic structure of the source zone.

The occurrence of aftershocks far from the main rupture can in principle be explained by additional static stress fields induced by the mainshock slip. As a matter

of fact, two comparatively simple sources were acting on the same fault: the main shock and the secondary flow, with different slip directions. Both these fields can be seen in the aftershock distribution. The aftershock area as a whole is elongate roughly along the maximum horizontal static stresses generated by the main shock. Similarly, the north-south aftershock band located north of the main rupture is elongate in the direction of the maximum stress generated by the secondary flow. In the latter case the model also accounts for the sign of the strain, namely, horizontal extension. This can be seen as follows. The aftershocks that occurred at crustal depths in the Vyvenka depression are located in the back of the allochthonous block (with respect to the main fault). If the slip had an upthrow component, then subhorizontal tension must have arisen in that area. It is of interest to note that a symmetrical pattern is not observed in the autochthonous block. This may indicate that it was only the allochthon which was active during the earthquake.

When using strain characteristics of the Khailino earthquake to deduce plate boundary kinematics, one should of course prefer the mainshock source parameters. Apart from scale considerations (a major earthquake, the maximum spatial averaging), it should once again be emphasized that the main shock occurred in a much more isotropic medium than the subsequent aftershocks, hence is a more direct reflection of the tectonic stress at this local segment of plate boundary. The mainshock parameters are consistent with northwest compression.

The chief conclusions and hypotheses based on seismological data are as follows.

1) The Khailino earthquake occurred in an area of dominant NW-SE compression and involved a crustal southeast reverse movement.

2) The earthquake did not lie on a major active fault, the resulting crustal fracture about 40 km long is a new dislocation.

3) The formation of the main fault, elongate at an angle of about 40 degrees with

respect to the slip direction, produced considerable strength anisotropy at the source.

4) The direction of subsequent slip (most of the larger aftershocks) was largely controlled by the shape of the weakened zone.

5) Most aftershocks were confined to the main fault and to the allochthonous block, a zone of horizontal compression starting to develop in the frontal part of the block (similarly to the main shock) and a zone of extension in the back of it.

Appendix 1. Derivation of equation (9)

The i-th Cartesian component of the displacement field $u_i(\mathbf{x},t)$ can be expressed by

$$u_i(\mathbf{x},t) = \int_\Omega dV_y \int_0^{\Delta t} \frac{\partial}{\partial y_l} H_{ij}(\mathbf{x},\mathbf{y},t-\tau)\dot{\Gamma}_{jl}(\mathbf{y},\tau)d\tau \tag{13}$$

where $(0,\Delta t)$ is the interval in which $\dot{\Gamma}_{jl}(\mathbf{y},\tau)$ is not identically zero, and $H_{ij}(\mathbf{x},\mathbf{y},t)$ is a time integral of Green's function:

$$H_{ij}(\mathbf{x},\mathbf{y},t) = \int_0^t G_{ij}(\mathbf{x},\mathbf{y},\tau)d\tau. \tag{14}$$

Replacing in (13) the function $H_{ij}(\mathbf{x},\mathbf{y},t-\tau)$ by its Taylor series in powers of $\mathbf{y}$ and in powers of τ, we get

$$u_i(\mathbf{x},t) = \sum_{m=0}^{\infty}\sum_{n=0}^{\infty} \frac{(-1)^n}{m!n!}\dot{\Gamma}^{(m,n)}_{jl;k_1\ldots k_m}(0,0)\frac{\partial^n}{\partial t^n}\frac{\partial}{\partial y_{k_1}}\cdots\frac{\partial}{\partial y_{k_m}}\frac{\partial}{\partial y_l}H_{ij}(\mathbf{x},\mathbf{y},t)\Big|_{y=0} \tag{15}$$

We use here this same notation for stress glut moments as in Backus, 1977. We have for the Fourier transforms $G_{ij}(\mathbf{x},\mathbf{y},\omega)$ and $H_{ij}(\mathbf{x},\mathbf{y},\omega)$ from (14):

$$H_{ij}(\mathbf{x},\mathbf{y},\omega) = \frac{1}{i\omega}G_{ij}(\mathbf{x},\mathbf{y},\omega) \tag{16}$$

Using formulae (15) and (16) we have for the Fourier transform $u_i(\mathbf{x},\omega)$:

$$u_i(\mathbf{x},\omega) = \sum_{m=0}^{\infty}\sum_{n=0}^{\infty} \frac{(-1)^n}{m!n!}\dot{\Gamma}^{(m,n)}_{jl;k_1\ldots k_m}(0,0)(i\omega)^{n-1}\frac{\partial}{\partial y_{k_1}}\cdots\frac{\partial}{\partial y_{k_m}}\frac{\partial}{\partial y_l}G_{ij}(\mathbf{x},\mathbf{y},\omega)\Big|_{y=0} \tag{17}$$

Taking into account the symmetry of coefficients $\frac{\partial}{\partial y_{k_1}}\cdots\frac{\partial}{\partial y_{k_m}}\frac{\partial}{\partial y_l}G_{ij}$ with respect to $k_1,\ldots,k_m$ and l, one can see that all elements of the moment $\dot{\Gamma}_{jl;k_1\ldots k_m}$ obtained by cyclic permutation of $k_1,\ldots,k_m$ and l are multiplied by the same coefficient in the right-hand side of (17). As a result, in the general case stress glut moments of spatial degree $m \geq 2$ are not uniquely determined by the displacement field (see Backus, 1977).

In the special case of a seismic source where (1) is valid we have for stress glut moments:

$$\dot{\Gamma}^{m,n}_{jl;k_1\ldots k_m} = M_{jl} f^{(m,n)}_{k_1\ldots k_m}. \tag{18}$$

From (17) and (18) we then have equation (9). One can see that moments $f^{(m,n)}_{k_1\ldots k_m}$ in (9) are symmetric with respect to $k_1,\ldots,k_m$. The coefficients $\frac{\partial}{\partial y_{k_1}}\cdots\frac{\partial}{\partial y_{k_m}}\left[M_{jl}\frac{\partial}{\partial y_l}G_{ij}(\mathbf{x},\mathbf{y},\omega)\,|_{y=0}\right]$ have the same symmetry.

So all different elements of the moment $f^{(m,n)}_{k_1\ldots k_m}$ are multiplied by different coefficients in the right-hand side of (9), and these elements are uniquely determined by the displacement flied $\mathbf{u}(\mathbf{x},\omega)$.

Appendix 2. Proof of inequality (11).

Let us consider a space of such functions $\psi(\mathbf{x},t)$ that integral

$$\int_\Omega dV_x \int_0^\infty f(\mathbf{x},t)\psi^2(\mathbf{x},t)dt$$

exists. Here $f(\mathbf{x},t)$ - non-negative function from (1), $\mathbf{x}=(x_1,x_2,x_3)$ - spatial vector and t - time. Let us define for this space a scalar product of functions $\varphi_i(\mathbf{x},t)$ and $\varphi_j(\mathbf{x},t)$ by the formula

$$(\varphi_i,\varphi_j) = \frac{1}{M_0}\int_\Omega dV_x \int_0^\infty f(\mathbf{x},t)\varphi_i(\mathbf{x},t)\varphi_j(\mathbf{x},t)dt, \tag{19}$$

where M_0- seismic moment.

Let us consider a linear span of independent functions φ_k, where $\varphi_k(\mathbf{x},t)=x_k$ $(k=1,2,3)$. Let $P(\mathbf{x},t)$ - projection of function $\psi(\mathbf{x},t)=t$ on this sub-space. Then for $P(\mathbf{x},t)$ we have

$$P(\mathbf{x},t) = c_i\varphi_i = c_i x_i = \mathbf{c}^T\mathbf{x} = \mathbf{x}^T\mathbf{c}, \tag{20}$$

where c_i is minimizing a product (q,q) defined by (13) and

$$q = t - c_i x_i = t - \mathbf{c}^T\mathbf{x}. \tag{21}$$

Taking into account that $\mathbf{x}=0$ and $t=0$ are spatial and temporal centroids of the source we will obtain following formulae for $\mathbf{c}$ and $P(\mathbf{x},t)$:

$$\mathbf{c} = \mathbf{W}^{-1}\mathbf{w}, \tag{22}$$

and

$$P(\mathbf{x},t) = \mathbf{x}^T\mathbf{W}^{-1}\mathbf{w}, \tag{23}$$

where $\mathbf{W}$ and $\mathbf{w}$ are defined by formulae (7) and (8).

The Bessel inequality gives us

$$(P,P) \le (t,t).$$

But $(t,t)=(\Delta\tau)^2$, and for (P,P) we have

$$\begin{aligned}(P,P) &= \frac{1}{M_0}\int_\Omega dV_x \int_0^\infty f(\mathbf{x},t)\mathbf{w}^T\mathbf{W}^{-1}\mathbf{x}\mathbf{x}^T\mathbf{W}^{-1}\mathbf{w}dt\\ &= \mathbf{w}^T\mathbf{W}^{-1}\mathbf{W}\mathbf{W}^{-1}\mathbf{w} = \mathbf{w}^T\mathbf{W}^{-1}\mathbf{w}.\end{aligned}$$

And finally

$$\mathbf{w}^T\mathbf{W}^{-1}\mathbf{w} \le (\Delta\tau)^2. \tag{24}$$

Inequality (24) is valid in the case of a 2-dimensional source region (a plane source) as well. Rewriting (24) in such a case in the coordinates of the main axes of the matrix $\mathbf{W}$, using formulae (4)-(8) we will obtain inequality (11).

REFERENCES

[1] Backus G., Mulcahy M., Moment tensors and other phenomenological descriptions of seismic sources. Pt.1. Continuous displacements, *Geophys. J. R. Astron. Soc.*, **46**, 341-362, 1976.

[2] Backus G., Interpreting the seismic glut moments of total degree two or less, *Geophys. J. R. Astron. Soc.*, **51**, 1-25, 1977.

[3] Bukchin B.G., Estimation of earthquake source parameters. In: Keilis-Borok V.I. (editor), Seismic surface waves in a laterally inhomogeneous earth, Dortrecht, Kluwer Academic Publishers. 229-245, 1989.

[4] Levshin A.L., Effects of lateral inhomogeneity on surface wave amplitude measurements, *Annales Geophysicae*, 3, 4, 511-518, 1985.

[5] Lander A.V., Bukchin B.G., Droznin D.V. and Kiryushin A.V., The tectonic environment and source parameters of the Khailino (Koryakiya) earthquake of March 8, 1991: Does a Beringia plate exist? (Submitted to *Computashinal seismology and geodynamics*, 26-27, 1994). measurements, *Annales Geophysicae*, 3, 4, 511-518, 1985.